

PAR Proteins Regulate Microtubule Dynamics at the Cell Cortex in *C. elegans*

Jean-Claude Labbé,* Paul S. Maddox,
E.D. Salmon, and Bob Goldstein
Department of Biology
The University of North Carolina at Chapel Hill
Chapel Hill, North Carolina 27599-3280

Summary

Background: The PAR proteins are known to be localized asymmetrically in polarized *C. elegans*, *Drosophila*, and human cells and to participate in several cellular processes, including asymmetric cell division and spindle orientation. Although astral microtubules are known to play roles in these processes, their behavior during these events remains poorly understood.

Results: We have developed a method that makes it possible to examine the residence time of individual astral microtubules at the cell cortex of developing embryos. Using this method, we found that microtubules are more dynamic at the posterior cortex of the *C. elegans* embryo compared to the anterior cortex during spindle displacement. We further observed that this asymmetry depends on the PAR-3 protein and heterotrimeric G protein signaling, and that the PAR-2 protein affects microtubule dynamics by restricting PAR-3 activity to the anterior of the embryo.

Conclusions: These results indicate that PAR proteins function to regulate microtubule dynamics at the cortex during microtubule-dependent cellular processes.

Introduction

The *C. elegans par* genes were identified through maternal-effect lethal genetic screens and have been shown to be required for establishing the initial anteroposterior axis of polarity in the early embryo [1–3]. While all PAR proteins are found at the cell cortex, some of them are localized to discreet regions along the anteroposterior axis of the embryo [4]. For instance, PAR-3, PAR-6, and PKC-3 are members of a protein complex and are localized at the anterior cortex of the embryo [5–7]. Likewise, the proteins PAR-1 and PAR-2 are present at the posterior cortex of the embryo [8, 9]. Localization of some of these proteins along the anteroposterior axis is mutually exclusive, as members of the anterior and posterior groups show little overlap in their localization, and the PAR-2 and PAR-3 proteins exclude each other from their respective cortices [4]. Therefore, PAR proteins define anterior and posterior cortical domains in the early *C. elegans* embryo.

Interest in the *par* genes has grown lately from reports showing that their functions are conserved in *Drosophila* and human cells [10]. In *Drosophila*, the *par* genes are required for polarity in the early embryo as well as in neuroblasts and neuroepithelial cells [11–13]. The *Dro-*

sophila PAR proteins are also localized to discreet regions of the cell cortex and may locally define and modulate the properties of cortices. In human cells, the PAR-3/PAR-6/PKC-3 protein complex has been localized at tight junctions and also has been shown to participate in cell polarity [14–16]. Nevertheless, the mechanisms by which PAR proteins establish polarity remains elusive.

Mutations in the *C. elegans par* genes result in phenotypes that include failure in several microtubule-dependent processes, including posterior spindle displacement, spindle rocking, and rotation of the nucleus/centrosome complex [4]. Because PAR proteins are localized at the cortex in early embryos, we were interested to find out whether they can regulate microtubule dynamics in a manner that might influence these cellular processes. We therefore examined the properties of astral microtubules in early wild-type and *par* mutant *C. elegans* embryos.

Results

Microtubules Are More Dynamic at the Posterior Cortex Compared to the Anterior

In order to characterize the effects of PAR proteins on microtubule dynamics during microtubule-dependent processes, we chose to study microtubule dynamics during the event of spindle positioning, as opposed to spindle rocking or rotation of the nuclear/centrosome complex, for the following reasons. First, microtubule-dependent cellular processes are associated with much intracellular movement, and spindle positioning displays the least movement among these, making it easier to monitor individual microtubules over time. Second, the PAR proteins are localized at the cortex along the anteroposterior axis of the embryo at the stage of spindle positioning, and the spindle remains oriented along the anteroposterior axis throughout all this process [4]; this stable orientation makes it easier to discriminate between populations of microtubules that interact with either the anterior or the posterior region of the cortex. And, third, recent spindle-severing experiments demonstrated that the PAR-2 and PAR-3 proteins regulate pulling forces on each side of the spindle during spindle positioning [17]; this finding indicates that PAR proteins are influencing microtubule-dependent processes at this stage. We determined that posterior spindle displacement occurs at metaphase: it starts 94 ± 4 s after pronuclear envelope breakdown and ends 50 ± 8 s later at the start of sister chromatid and centrosome separation at anaphase B ($n = 5$ embryos; see Figure S1 in the Supplemental Data available with this article online).

We first attempted to quantify microtubule dynamics by imaging microtubules in a middle plane of wild-type embryos and quantifying the length of time during which each microtubule could be seen in the plane of focus (data not shown). However, because microtubules enter and leave the plane of focus in these time-lapse images, this approach could not discriminate between microtu-

*Correspondence: jeanclaude.labbe@bc.biol.ethz.ch

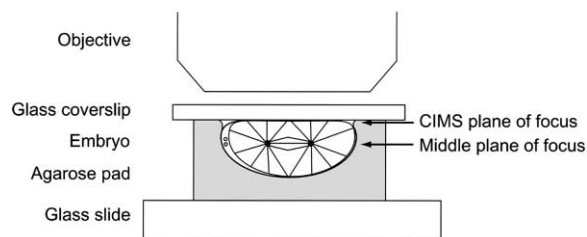


Figure 1. Diagram of the Mounting Method for Cortical Imaging of Microtubule Stability

Flattening of the upper surface of the embryo allows the visualization of both anterior and posterior regions of the cortex. Such flattening reduces the thickness of the embryo from 30 μm to approximately 20 μm . See the main text for further details.

bules that shorten and those that leave the plane of focus and was therefore not suitable to accurately quantify microtubule dynamics.

We therefore devised an approach to directly assess the stability of individual microtubules at the cortex. Embryos were mounted on agarose pads as described previously [18]. In this method, applying a coverslip flattens the upper surface of each embryo (Figure 1; see the Experimental Procedures). Focusing near the coverslip allowed the simultaneous imaging of both the anterior and posterior cortex, where the pulling force-modulating proteins PAR-3 and PAR-2, respectively, are localized [17, 19]. Monitoring microtubule properties in these regions of the cortex is relevant because pulling forces are active at these sites (S. Grill and T. Hyman, personal communication; J.-C.L. and B.G., unpublished data). By this method, tips of microtubules at the cortex are visible as individual dots or short line segments of fluorescence, while microtubules that shorten away from the cortex are no longer visible (Figures 2A and 2B). Although microtubules could also disappear from the plane of focus by being severed at the centrosome and depolymerized along their entire length while remaining attached to the cortex, analysis of individual time-lapse images at the middle plane revealed little or no microtubule severing at the centrosome between the events of pronuclear envelope breakdown and the start of anaphase (data not shown). Imaging at the cell cortex has the advantage of assessing directly the presence of individual microtubules at the anterior and posterior cortex in the same embryo, and it eliminates the problem of microtubules going in and out of the plane of focus.

Microtubule residence time at the cortex was quantified by two methods (see the Experimental Procedures): a direct method that relies on counting the length in time during which each microtubule is present at the cortical plane in a time-lapse series of images (Table 1 and Figure S2), and an indirect method that depends on kymocube analysis in given sections of cortex (Figure S3 and Table S1). The indirect method has the advantage of facilitating the quantification of the residence times of large numbers of microtubules. However, we expected this method to produce consistent underestimates of true residence time, since this method excludes dimly fluorescent time segments as well as microtubules that enter and leave the kymocube section

during the time of analysis; this appears to be the case (compare methods in Tables 1 and S1). Since the residence times estimated by the indirect method were statistically indistinguishable between independent observers (data not shown), and nearly all of the differences found between specific conditions were found by using both the direct and indirect methods (Tables 1, 2, and S1), we conclude that both methods are valid means of comparing microtubule residence times at the cortex, although only the direct method produces the true residence times. Although our approach does not allow us to visualize all aspects of microtubule dynamic instability, it enables us to determine how long microtubules interact with the cortex and thus to assess this aspect of their dynamic state.

We quantified microtubule residence time at the cortex by using this approach and found a difference in stability between anterior and posterior microtubules during posterior spindle displacement. As shown in Figure 3, anterior microtubules stayed at the cortex for an average of 16.5 ± 1.0 s, while posterior microtubules stayed at the cortex for 14.5 ± 0.6 s (mean \pm SE over ten embryos); this difference is statistically significant ($p < 0.05$; Table 1). These results indicate that anterior microtubules reside at the cortex on average 15% longer than posterior microtubules. For convenience, we refer to our imaging approach as CIMS, for cortical imaging of microtubule stability.

The PAR Proteins Regulate Microtubule Dynamics at the Cortex

The fact that microtubules are more stable at the anterior cortex of the embryo during posterior spindle displacement suggested that PAR proteins could regulate microtubule stability. We set out to test this more directly by looking at microtubule stability in polarity-defective embryos, mutant for either *par-1*, *par-2*, or *par-3*, in which posterior spindle displacement is compromised [19]. The localization of the PAR-2 and PAR-3 proteins at the cortex is mutually exclusive, and disrupting the function of either protein causes the other one to spread uniformly around the cortex [4]. The protein PAR-1, which contains motifs found in microtubule affinity-regulating kinases (MARKs) [20], also shows different localization patterns in *par-2* and *par-3* mutant backgrounds: in *par-3* mutant embryos, the PAR-1 protein is present uniformly at the anterior and posterior cortex, while, in *par-2* mutants, PAR-1 is not localized at the cortex [4].

We quantified the residence time of microtubules at the cortex by CIMS in wild-type *par-1(RNAi)*, *par-2(RNAi)*, and *par-3(RNAi)* embryos at the time that posterior spindle displacement normally occurs in wild-type. In wild-type embryos, the position of the sperm pronucleus defines the posterior [21]. Because *par* mutants fail to establish proper embryonic polarity, we defined the posterior side of the embryo as the pole where the sperm pronucleus was visible before the pronuclei met. We first quantified microtubule stability at the cortex of *par-1(RNAi)* embryos, in which the spindle still moves posterior, albeit to a lesser extent than in wild-type embryos (see the Experimental Procedures). As shown in Figure 3, disrupting the function of *par-1* had slight effects on microtubule dynamics, but the residence time

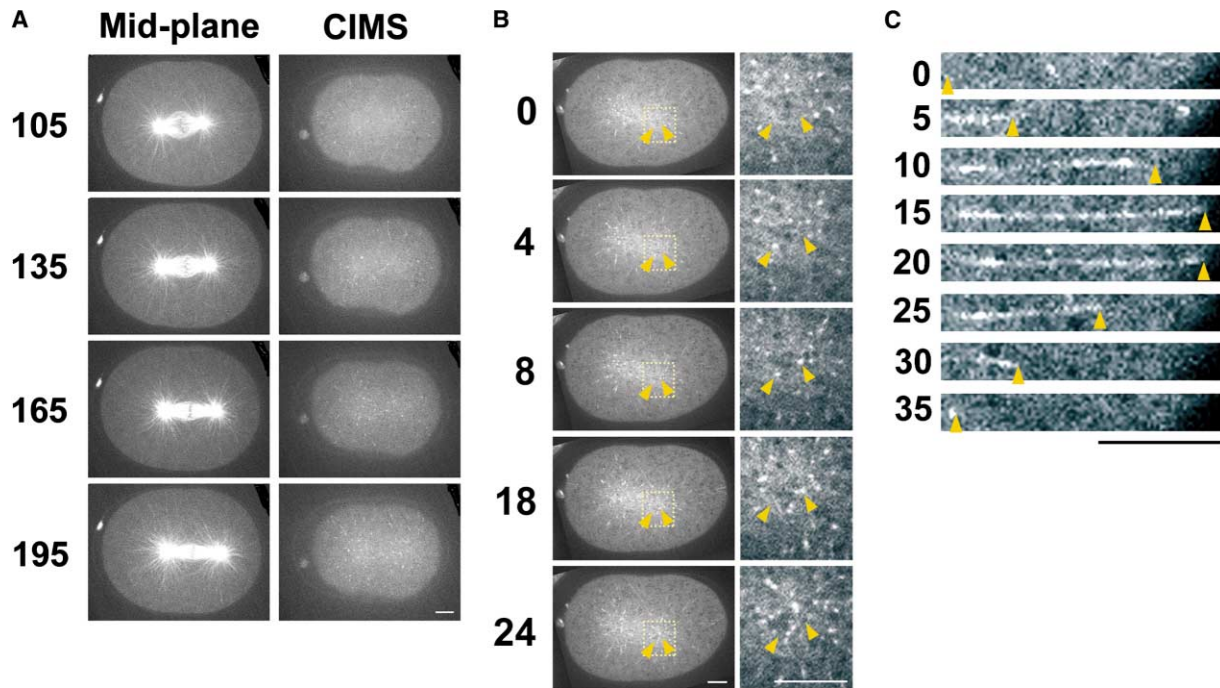


Figure 2. Cortical Imaging of Microtubule Stability in Wild-Type Embryos

(A) Time-lapse images at mid- (left column) and cortical (right column) planes of wild-type embryos expressing α -tubulin::gfp. In CIMS, microtubules are visible as individual dots or short line segments of fluorescence. The numbers on the left represent time (in seconds) after pronuclear envelope breakdown.

(B) Time-lapse images were acquired to assess microtubule stability by CIMS. The images in the right-hand column are magnifications of the yellow, boxed portion in the images in the left-hand column. In each frame, the two arrowheads indicate individual microtubules that enter and leave the cortex in this series of time-lapse images. The numbers on the left represent time (in seconds) relative to the first frame of this series.

(C) Individual microtubule growth and shortening at the cell cortex. In CIMS, it is sometimes possible to visualize the dynamic behavior of individual microtubules. This could be due to the fact that a small population of growing microtubules sometimes bend at the cortex and continue to grow along this plane. These events are rare and do not represent the vast majority of microtubules, which do not have such behavior. Arrowheads mark the position of a microtubule end in these time-lapse images. Numbers on the left represent time (in seconds) relative to the first frame of this series.

In all panels, anterior is oriented toward the left, and each scale bar represents 5 μ m.

Table 1. Average Stability of Microtubules in Wild-Type, Polarity-Defective, and Spindle Positioning-Defective Embryos

Background	Average Microtubule Residence Time at the Cortex in Seconds (n)			Difference (Anterior versus Posterior) ^a	p Value (Anterior versus Posterior) ^b
	Anterior	Posterior	Whole Embryo		
Wild-Type	16.5 \pm 1.0 (199)	14.5 \pm 0.6 (198)	15.5 \pm 0.8 (397)	13.8%	p = 0.03
<i>par-1(RNAi)</i>	15.6 \pm 1.5 (139)	13.1 \pm 0.9 (139)	14.4 \pm 1.2 (278)	19.1%	p = 0.02
<i>par-2(RNAi)</i>	15.8 \pm 0.8 (151)	15.7 \pm 0.8 (151)	15.7 \pm 0.7 (302)	0.6%	p = 0.85
<i>par-3(RNAi)</i>	13.4 \pm 1.2 (142)	13.3 \pm 0.7 (142)	13.3 \pm 0.9 (284)	0.8%	p = 0.96
<i>par-2(RNAi); par-3(RNAi)</i>	12.3 \pm 0.6 (164)	12.4 \pm 0.8 (164)	12.3 \pm 0.7 (328)	0.8%	p = 0.75
<i>Gα(RNAi)^c</i>	14.8 \pm 1.0 (150)	14.4 \pm 1.1 (150)	14.6 \pm 1.0 (300)	2.8%	p = 0.58
<i>Gα(RNAi); par-2(RNAi)^c</i>	15.1 \pm 1.2 (152)	16.0 \pm 1.3 (152)	15.5 \pm 1.2 (304)	5.6%	p = 0.31
<i>Gα(RNAi); par-3(RNAi)^c</i>	13.0 \pm 0.6 (156)	13.2 \pm 0.9 (156)	13.1 \pm 0.7 (312)	1.5%	p = 0.80

Microtubule stability was determined by cortical imaging of microtubule stability (CIMS) and was quantified by using method 1 (see the Experimental Procedures). Each value corresponds to the average residence time of microtubules at the cortex \pm the standard error of the mean across ten embryos. The number given in parentheses corresponds to the total number of microtubules monitored. Microtubules were highly dynamic on each side of the spindle, and their residence time at the cortex ranged from 4 to 60 s. The standard deviation for total microtubule residence time at the cortex in all backgrounds was 7.3 s and ranged from 4.6 s to 10.0 s depending on the background.

^a Represents the percentage of increase in stability at the cortex of anterior microtubules compared to posterior microtubules.

^b p values from paired Student's t tests between anterior and posterior average microtubule residence time at the cortex. Values were considered significantly different if p < 0.05.

^c *G α (RNAi)* corresponds to the simultaneous disruption of the *goa-1* and *gpa-16* genes. See the main text for details.

Table 2. Statistical Comparison of Microtubule Residence Time at the Cortex between Various RNAi Backgrounds

Background Compared	p Value (Method 1) ^a	p Value (Method 2) ^a
Wild-type (anterior) versus <i>par-1(RNAi)</i> (anterior)	p = 0.254	p = 8.907E⁻⁵
Wild-type (posterior) versus <i>par-1(RNAi)</i> (posterior)	p = 0.037	p = 5.428E⁻¹¹
<i>par-2(RNAi)</i> versus <i>par-3(RNAi)</i>	p = 1.064E⁻⁴	p = 3.442E⁻⁵
<i>par-2(RNAi)</i> versus <i>par-2(RNAi); par-3(RNAi)</i>	p = 6.407E⁻¹¹	p = 1.530E⁻³
<i>par-2(RNAi)</i> versus $G_{\alpha}(RNAi)$	p = 0.171	p = 0.174
<i>par-2(RNAi)</i> versus $G_{\alpha}(RNAi); par-2(RNAi)$	p = 0.523	p = 0.085
<i>par-2(RNAi)</i> versus $G_{\alpha}(RNAi); par-3(RNAi)$	p = 9.809E⁻⁶	p = 9.737E ⁻³
<i>par-3(RNAi)</i> versus <i>par-2(RNAi); par-3(RNAi)</i>	p = 0.021	p = 0.402
<i>par-3(RNAi)</i> versus $G_{\alpha}(RNAi)$	p = 0.027	p = 3.978E⁻⁷
<i>par-3(RNAi)</i> versus $G_{\alpha}(RNAi); par-2(RNAi)$	p = 1.156E⁻³	p = 6.544E⁻⁸
<i>par-3(RNAi)</i> versus $G_{\alpha}(RNAi); par-3(RNAi)$	p = 0.723	p = 0.134
<i>par-2(RNAi); par-3(RNAi)</i> versus $G_{\alpha}(RNAi)$	p = 6.994E⁻⁶	p = 2.714E⁻⁵
<i>par-2(RNAi); par-3(RNAi)</i> versus $G_{\alpha}(RNAi); par-2(RNAi)$	p = 4.735E⁻⁹	p = 5.848E⁻⁶
<i>par-2(RNAi); par-3(RNAi)</i> versus $G_{\alpha}(RNAi); par-3(RNAi)$	p = 0.041	p = 0.535
$G_{\alpha}(RNAi)$ versus $G_{\alpha}(RNAi); par-2(RNAi)$	p = 0.438	p = 0.726
$G_{\alpha}(RNAi)$ versus $G_{\alpha}(RNAi); par-3(RNAi)$	p = 8.037E ⁻³	p = 2.305E⁻⁴
$G_{\alpha}(RNAi); par-2(RNAi)$ versus $G_{\alpha}(RNAi); par-3(RNAi)$	p = 1.661E⁻⁴	p = 5.651E⁻⁵

^ap values from Student's t tests (unpaired, homoscedastic) were obtained by comparing individual microtubule stability between various backgrounds by using the Bonferroni method of multiple comparisons. Because 17 comparisons were made for each method, values were considered significantly different if $p < 2.941E^{-3}$ (0.05/17). The p values that were statistically significant are in bold. See the Experimental Procedures for a description of methods 1 and 2.

of microtubules at the anterior cortex was on average 17% longer than at the posterior cortex, much as in wild-type. This suggests that, although PAR-1 may have a global effect on microtubule stability, perhaps through unlocalized PAR-1 present in the central cytoplasm [8], it might not function as an asymmetrically localized MARK in *C. elegans* embryos; we cannot exclude, however, that PAR-1 might depolymerize microtubules while they remain attached to the cell cortex, thus contributing to the posterior displacement of the spindle.

Disrupting the function of *par-2* or *par-3* resulted in changes in microtubule dynamics at the cortex. In both backgrounds, anterior and posterior microtubules had equal residence time at the cortex (Figure 3). This indicates that PAR-2 and PAR-3 are required for the asymmetric regulation of microtubule dynamics at the cortex in *C. elegans* embryos. Furthermore, the residence time at the cortex of microtubules in *par-2(RNAi)* embryos was on average 14% longer than in *par-3(RNAi)* embryos (Tables 1 and 2), which suggests that PAR-2 and PAR-3 proteins have opposite effects on microtubule stability.

In order to assess whether PAR-2 affects microtubule dynamics by altering the localization of PAR-3, or vice versa, we quantified the residence time of microtubules at the cortex in embryos in which the function of both *par-2* and *par-3* was disrupted simultaneously. We found that microtubule residence time at the cortex in the double *par-2(RNAi); par-3(RNAi)* is similar to *par-3(RNAi)* single embryos (Table 2 and Figure 3). This suggests that PAR-3 is required to stabilize microtubules, and that the effect of PAR-2 on microtubule stability likely occurs through excluding PAR-3 from the posterior cortex of the embryo. This is consistent with previous results that demonstrated that *par-3* is epistatic to *par-2* for centrosome rotation and spindle orientation in the 2-cell embryo [22]. Taken together, these results indicate that PAR-3 participates in the regulation of microtubule dynamics at the cortex in a way that is independent of *par-1* activity, and that PAR-2 affects micro-

tubule stability by restricting PAR-3 activity to the anterior of the embryo.

Heterotrimeric G Protein Signaling Influences Microtubule Dynamics at the Cortex

Heterotrimeric G protein signaling was recently shown to be involved in asymmetric cell division in both *C. elegans* and *Drosophila* [23, 24]. In the early *C. elegans* embryo, disrupting simultaneously the function of two genes encoding G_{α} subunits (*goa-1(RNAi); gpa-16(RNAi)*, hereafter referred to as $G_{\alpha}(RNAi)$) causes a failure of posterior spindle displacement, resulting in two cells of equal size after cytokinesis [24]. In $G_{\alpha}(RNAi)$ embryos, the localization of PAR-2 and PAR-3 proteins is unaffected and polarity is normal, indicating that G proteins affect spindle position downstream of the PAR proteins [24]. This is similar to the situation in *Drosophila* neuroblasts, where heterotrimeric G protein signaling is also required downstream of Bazooka (Baz), a PAR-3 homolog, for asymmetric cell division [25]. While G_{α} was found to be localized symmetrically at the cortex and on asters in a *C. elegans* embryo [24], it is localized asymmetrically at the apical cortex of *Drosophila* neuroblasts and at the anterior cortex of sensory organ precursor cells [25]; this finding suggests at least some differences in the regulation of G protein signaling in these organisms. We asked whether heterotrimeric G protein signaling regulates microtubule dynamics at the cortex in *C. elegans*. We quantified microtubule residence time at the cortex by CIMS in $G_{\alpha}(RNAi)$ embryos and found that anterior and posterior microtubules have equal stability at the cortex when the function of G_{α} is disrupted (Table 1 and Figure 3). This indicates that G protein activity is required to asymmetrically regulate microtubule dynamics in *C. elegans* embryos.

The average residence time of microtubules at the cortex in $G_{\alpha}(RNAi)$ embryos was not consistently different from that of microtubules in *par-2(RNAi)* or *par-3(RNAi)* embryos (compare p values from methods 1

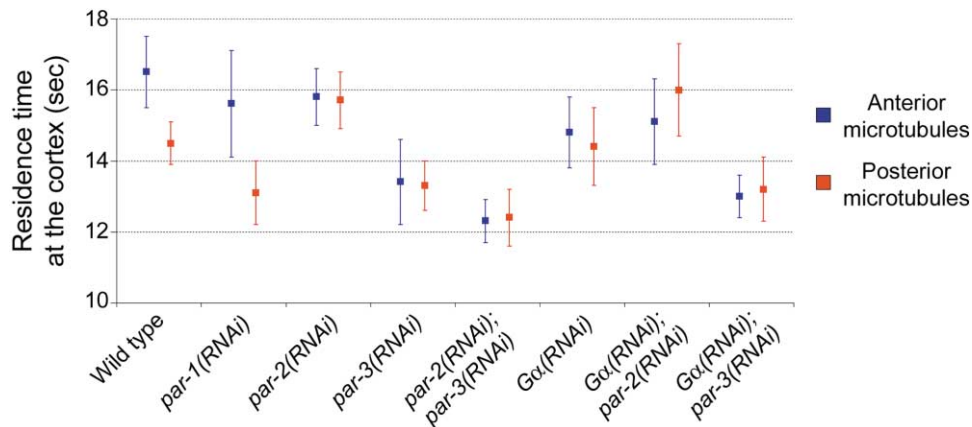


Figure 3. Stability of Microtubules at the Cortex in Wild-Type and Spindle Positioning-Defective *C. elegans* Embryos

The residence time at the cortex of microtubules at the anterior (blue) and posterior (red) cortex was determined for ten embryos in each background. Each value corresponds to the average residence time at the cortex (in seconds) \pm standard error of the mean across ten embryos. Statistically significant differences between each background are shown in Table 1 and Figures S1 and S2.

and 2 in Table 2), and these similar residence times make it difficult to propose a clear epistasis pathway between PAR protein and G protein signaling for the regulation of microtubule stability at the cortex. We therefore addressed whether the difference in microtubule stability that we found between *par-2(RNAi)* and *par-3(RNAi)* embryos is dependent on $G\alpha$, by quantifying microtubule stability at the cortex in embryos in which the function of $G\alpha$ was disrupted in combination with either *par-2* or *par-3*. As shown in Figure 3, we observed that disrupting *par-2* or *par-3* function in combination with $G\alpha$ had effects on microtubule stability that suggest that PAR proteins affect microtubules independently of G protein signaling: the difference in microtubule stability at the cortex between $G\alpha(RNAi); par-2(RNAi)$ and $G\alpha(RNAi); par-3(RNAi)$ was on average 15%, similar to the difference in microtubule stability found between embryos where the function of *par-2* and *par-3* was disrupted individually ($p < 0.05$; Tables 1 and 2). Taken together, these results indicate that $G\alpha$ and PAR-3 regulate microtubule dynamics at the cortex, in manners that are at least partially independent.

Discussion

We have shown that microtubules are more stable at the anterior than the posterior cortex in wild-type *C. elegans* embryos. We have also shown that this difference in microtubule stability at the cortex is independent of the protein PAR-1 but depends on the proteins PAR-2, PAR-3, and $G\alpha$. A role for PAR-3 in microtubule anchoring or stabilization had been hypothesized previously, based on observations of defects in spindle orientation and spindle positioning of *par-3* mutant embryos [5, 17, 22]. Based on our results, we propose that PAR-3 stabilizes microtubules and that PAR-2 affects microtubule stability by restricting PAR-3 activity to the anterior of the embryo. Because disruption of $G\alpha$ does not yield results that are consistently distinguishable from those obtained by disruption of *par-2* or *par-3* (by using each of our methods of analysis), we cannot clearly ascribe a role for $G\alpha$ in stabilizing or destabilizing microtubules.

However, the fact that disruption of $G\alpha$ results in equal microtubule residence time at the anterior and posterior cortex clearly indicates that $G\alpha$ is required for asymmetric regulation of microtubule stability at the cortex. In *C. elegans*, *Drosophila*, and human cells, PAR-3 is found in a complex along with PAR-6, a protein with PDZ motifs, and an atypical protein kinase C, PKC-3 [10]. In *C. elegans* embryos, disruption of any individual member of this protein complex causes the mislocalization of the other members [7], and therefore it is currently not possible to directly test whether PAR-3 affects microtubule stability through the activity of PKC-3 or not. It will be of interest to determine whether microtubule dynamics at the cortex are regulated by atypical protein kinase C activity, as well as to identify whether this kinase can directly target microtubule-associated proteins (MAPs) to affect microtubule stability. PAR-6 also interacts with CDC-42 in *C. elegans* [26] and in human cells [14–16]. It is possible that the GTPase activity of CDC-42 could also directly or indirectly affect MAPs to modulate microtubule dynamics. Likewise, the DEP domain-containing protein LET-99 might affect the stability of microtubules at the posterior cortex of the embryo [27].

Our results demonstrate that PAR proteins and G protein signaling regulate microtubule dynamics at the cortex during spindle positioning in the early *C. elegans* embryo and are responsible for a $\sim 15\%$ difference in microtubule stability between the anterior and posterior cortices. This $\sim 15\%$ difference, although small, could perhaps contribute to posterior spindle displacement. Spindle-cutting experiments by Grill et al. estimated that pulling on the posterior aster is 40% stronger than on the anterior aster during posterior spindle displacement [17]. The regulation of microtubule dynamics along the anteroposterior axis of the embryo could modulate these pulling forces to influence posterior spindle displacement, a mechanism that has previously been proposed by Grill et al. from computer simulation experiments [17]. One possibility that is consistent with current data is that a limiting number of motor proteins, such as dynein motors, are present at the cell cortex to pull a fraction of the microtubules, and decreasing the stabil-

ity of microtubules in the posterior eliminates microtubules that do not engage dyneins. Such unengaged microtubules might obstruct pulling forces and impede movement of the spindle. In this regard, the large subunit of dynein (DHC-1) has been shown to localize to the entire cell cortex during metaphase and anaphase [28]; however, whether active DHC-1 is present in limiting concentrations in the cortex has yet to be determined. Alternatively, asymmetrically localized minus end-directed motor activity at the cortex of the embryo might itself locally influence microtubule dynamics, and the difference in microtubule stability at the cortex that we observed might be a consequence of an asymmetry in motor activity. PAR proteins and G proteins also influence other microtubule-dependent processes in the embryo, such as spindle rocking and centrosome rotation at the 2-cell stage [24]. The asymmetry in microtubule stability at the cortex that we observed might also contribute to the regulation of these processes. In the case of centrosome rotation, previous experiments demonstrated that this process is sensitive to pharmacological agents that either stabilize or destabilize microtubules [29]. This suggests that microtubule dynamics are important during this process.

We have measured an average microtubule residence time at the cortex of 15.5 ± 0.8 s in wild-type embryos (Table 1). If microtubules were continuously growing during this time, this would generate pushing force on the cortex. A microtubule pushing-based model was recently proposed to explain nuclear positioning in *S. pombe*. In this case, plus-end microtubule growth generates pushing force toward the minus-end and causes microtubule buckling in the cytoplasm [30]. We observed little, if any, buckling of microtubules during posterior spindle displacement in *C. elegans* embryos. Furthermore, Grill et al. reported pulling forces on astral microtubules [17]. These results suggest that microtubule plus-ends that interact with the cortex are stalled (not growing) and under tension. This raises the possibility that the microtubule plus-ends behave differently in the cytoplasm than they do when they make contact with the cell cortex.

Finally, we have described a novel approach, CIMS, to study the cortical stability of individual microtubules in a developmental system. Until now, most measurements of microtubule dynamics in vivo were done by using cells in culture or other relatively flat cells [31–34], which are better suited to image microtubules in a single plane of focus. We have used CIMS to study microtubule stability at the cortex of *C. elegans* embryos, which have a thickness of 20–30 μm . One of the main advantages of CIMS is that it reduces the imaging of a thick specimen to a thin region near the cell cortex. Therefore, it eliminates the problem of microtubules going in and out of the plane of focus. It also maximizes the optical resolution of fluorescence events by imaging near the objective lens, not deep into the specimen where light scattering occurs and thus optical resolution is decreased [35]. Furthermore, it is possible to use CIMS to visualize certain microtubules along their lengths and thus quantify additional aspects of their dynamic behavior in living embryos (Figure 2C). In preliminary experiments using this approach, we have determined an aver-

age growth rate of 35.7 ± 9.5 $\mu\text{m}/\text{min}$ ($n = 7$) and a shortening rate of 31.8 ± 12.2 $\mu\text{m}/\text{min}$ ($n = 5$) for microtubules at the cortex of *C. elegans* embryos undergoing mitosis. These rates are faster than those measured for microtubules in cultured cells but are similar to those observed in clarified *Xenopus* egg extracts [36]. CIMS may prove useful for studying microtubule dynamics in other thick biological specimens, such as *Drosophila*, *Xenopus*, and echinoderm embryos.

Conclusions

We conclude that PAR proteins and G protein signaling regulate the stability of individual microtubules at the cortex of *C. elegans* embryos. This indicates that proteins that regulate asymmetric cell division also modulate microtubule dynamics at the cell cortex.

Experimental Procedures

General Methods and Strains

C. elegans strains were cultured as described previously [37]. The wild-type strain used was the Bristol N2 strain. The strain TH2 contains an extrachromosomal array that consists of the gene coding for α -tubulin inserted in frame with *gfp*, under the control of the *pie-1* promoter [38]. This construct expresses an α -tubulin::GFP fusion protein in the *C. elegans* germline and thus maternally provides the fusion protein to maturing oocytes. This strain was grown at 25°C and was maintained by picking animals that express GFP in their germline and embryos, as determined by using a Zeiss SV11 stereomicroscope equipped with a HBO100 fluorescence illumination system (Carl Zeiss Microscopy).

RNA Interference

Disruption of *par-1*, *par-2*, *par-3*, *goa-1*, and *gpa-16* function was done by double-stranded RNA-mediated interference (RNAi) [39], and experiments were performed by injecting double-stranded RNA (dsRNA) molecules prepared as described previously [40]. RNAi disruption of *par-1*, *par-2*, and *par-3* recapitulated all the phenotypes that have been reported to be associated with loss of function of these genes (defects in spindle positioning, centrosome rocking and flattening, nucleus/centrosome rotation at the 2-cell stage; [1, 4]). We observed that the spindle in *par-1(RNAi)* embryos was positioned asymmetrically ($56\% \pm 2\%$ embryonic length, $n = 4$), albeit not as asymmetric as in wild-type embryos ($59\% \pm 1\%$ embryonic length, $n = 5$), despite showing all other *par-1* phenotypes (lethality, incorrect segregation of P granules, aberrant anterior centrosome rocking, synchronous second division; [4]). To address this issue, we measured the position of the spindle in *par-1(it51)* embryos, which produce a PAR-1 kinase-dead protein and have been shown to be strong alleled [8], and we also observed asymmetry in spindle positioning ($54\% \pm 2\%$ embryonic length, $n = 6$). Similar results were obtained when *par-1* dsRNA was injected into *par-1(it51)* mutants. This is consistent with previous results demonstrating that the spindle is positioned at $57\% \pm 2\%$ embryonic length in wild-type embryos and $53\% \pm 2\%$ embryonic length in *par-1(b274)* embryos [1]. In similar assays, we observed that the spindle in both *par-2(RNAi)* and *par-3(RNAi)* embryos was positioned symmetrically ($49\% \pm 1\%$ embryonic length, $n = 4$ for *par-2*; $49\% \pm 1\%$ embryonic length, $n = 5$ for *par-3*).

Imaging and Analysis

For the visualization of microtubules in live specimens, embryos were obtained by cutting open gravid hermaphrodites by using two 25G needles. Embryos were handled individually and were mounted on a coverslip coated with 1% poly-L-lysine in 1 μl egg buffer [41]. The coverslip was placed on a 3% agarose pad, and the edge was sealed with petroleum jelly. This mounting method has been shown previously to be compatible with normal development and thus does not disrupt cellular processes [18]. Time-lapse images were acquired by using a CS10 Yokogawa spinning-disk confocal system

(Perkin-Elmer Life Sciences Wallac) mounted on a Nikon Eclipse TE300 inverted microscope (Nikon Instrument Group). The specimens were illuminated at 488 nm with an air-cooled Ar/Kr laser (60 mW, Melles Griot). Digital images were acquired with an Orca ER Hamamatsu 16-bit cooled CCD camera (Hamamatsu Photonics), and the acquisition system was controlled by MetaMorph software (Universal Imaging). Fluorescence images were acquired with 350 ms exposure at 2- or 5-s intervals by using a Plan Apochromat 100×/1.4 NA objective and 2 × 2 binning in the camera. Images were analyzed by using MetaMorph software and Microsoft Excel (Microsoft) and were processed with Adobe Photoshop (Adobe Systems).

Microtubule residence time at the cortex was quantified by using two methods. In method 1, a given individual fluorescent dot was chosen at random in a time-lapse image from a series, and the movie was played back and forth to determine the precise time-lapse images during which the fluorescent dot was visible (when the microtubule appears and disappears from the plane of focus). Because the frames were taken 2 s apart, the number of frames in which the dot was visible was multiplied by two to obtain the number of seconds during which this microtubule remained in the plane of focus. To ensure representative counts, microtubules were chosen from all regions of the anterior and posterior cortices and throughout the time between pronuclear envelope breakdown and the start of anaphase. To avoid quantifying spurious fluorescence events, fluorescent dots that were only present in a single frame were excluded from analysis. See Figure S2 and Movie 3 for examples of this method. The stability of a minimum of 24 microtubules was averaged for each embryo, and 10 embryos were monitored for each condition.

In method 2, a 2.4 μm high rectangular region was selected in the middle of the embryo. This region extended from the anterior to the posterior end of the embryo. The time-lapse images corresponding to this region were equalized (by using average fluorescence intensity as a reference) to correct for fluorescence photobleaching that occurs during the filming procedure. The height of each equalized time-lapse image was then compressed (by maximal intensity) to a four pixel-wide line, and these time-lapse lines were combined together (using the “three-dimensional reconstruction” algorithm in MetaMorph and selecting a 90° angle view), thereby generating a composite image (termed a kymocube) that contains anterior-posterior information along the x axis and time along the y axis (see Figure S3). In these kymocubes, microtubules at the cortex can be visualized as lines extending along the time axis. An automatic threshold (in MetaMorph software) was then applied to select for the brightest fluorescence events. Microtubule residence time at the cortex was then determined by measuring the length of individual, continuous lines in each processed kymocube and converting them to the appropriate number of seconds. Because this method excludes dimly fluorescent segments, it likely underestimates the residence time of microtubules at the cortex; nevertheless, results obtained with this method could be reproduced by blind analysis. A total of three rectangular regions were selected from each half embryo (5 embryos of each background were examined), and the residence time at the cortex of 15 microtubules was quantified for each side of the embryo per rectangular region (45 microtubules quantified for each side of each embryo).

We observed that robust posterior centrosome rocking typically occurred after the start of anaphase, and that weak rocking was detectable starting 10 ± 10 s (n = 5 embryos) before anaphase onset, at the end of our time window (144 ± 8 s) for measuring microtubule residence time at the cortex. Excluding our measurements of microtubule stability at the cortex during this 10 ± 10 s did not significantly affect our results (data not shown). Therefore, lateral rocking of the posterior centrosome does not significantly contribute to the difference in microtubule stability at the cortex observed between anterior and posterior regions of the embryo.

Supplemental Data

Supplemental Data including three figures, a table, and three movies are available at <http://images.cellpress.com/supmat/supmatin.htm>.

Acknowledgments

We are grateful to Karen Oegema and Tony Hyman for providing the *α-tubulin::gfp*-expressing strain, Monica Gotta and Julie Ahringer for providing the *goa-1* and *gpa-16* DNA constructs, Stephan Grill and Tony Hyman for sharing unpublished results, John Fricks for help with statistical analysis, and Kerry Bloom and Chad Pearson for critical reading of the manuscript. We would also like to thank Joe Kearney, Dale Beach, and all members of the Goldstein, Salmon, and Bloom labs for helpful discussions and technical advice. Some strains used in this work were provided by the *Caenorhabditis* Genetics Center, which is funded by the National Center for Research Resources of the National Institutes of Health (NIH). This work was supported by postdoctoral fellowships from le Fonds pour la Formation de Chercheurs et l'Aide à la Recherche (Québec) and le Conseil de Recherches en Sciences Naturelles et en Génie du Canada to J.-C.L., NIH grant GM60678 to E.D.S., and a March of Dimes Basil O'Connor Starter Scholar Award to B.G. B.G. is a Pew Scholar in the Biomedical Sciences.

Received: January 15, 2003

Revised: February 26, 2003

Accepted: February 28, 2003

Published: April 29, 2003

References

- Kemphues, K.J., Priess, J.R., Morton, D.G., and Cheng, N.S. (1988). Identification of genes required for cytoplasmic localization in early *C. elegans* embryos. *Cell* 52, 311–320.
- Watts, J.L., Etemad-Moghadam, B., Guo, S., Boyd, L., Draper, B.W., Mello, C.C., Priess, J.R., and Kemphues, K.J. (1996). *par-6*, a gene involved in the establishment of asymmetry in early *C. elegans* embryos, mediates the asymmetric localization of PAR-3. *Development* 122, 3133–3140.
- Morton, D.G., Shakes, D.C., Nugent, S., Dichoso, D., Wang, W., Golden, A., and Kemphues, K.J. (2002). The *Caenorhabditis elegans par-5* gene encodes a 14-3-3 protein required for cellular asymmetry in the early embryo. *Dev. Biol.* 241, 47–58.
- Kemphues, K.J., and Strome, S. (1997). Fertilization and establishment of polarity in the embryo. In *C. elegans* II, D. Riddle, T. Blumenthal, B.J. Meyer, and J.R. Priess, eds. (Cold Spring Harbor, NY: Cold Spring Harbor Laboratory Press), pp. 335–359.
- Etemad-Moghadam, B., Guo, S., and Kemphues, K.J. (1995). Asymmetrically distributed PAR-3 protein contributes to cell polarity and spindle alignment in early *C. elegans* embryos. *Cell* 83, 743–752.
- Tabuse, Y., Izumi, Y., Piano, F., Kemphues, K.J., Miwa, J., and Ohno, S. (1998). Atypical protein kinase C cooperates with PAR-3 to establish embryonic polarity in *Caenorhabditis elegans*. *Development* 125, 3607–3614.
- Hung, T.J., and Kemphues, K.J. (1999). PAR-6 is a conserved PDZ domain-containing protein that colocalizes with PAR-3 in *Caenorhabditis elegans* embryos. *Development* 126, 127–135.
- Guo, S., and Kemphues, K.J. (1995). *par-1*, a gene required for establishing polarity in *C. elegans* embryos, encodes a putative Ser/Thr kinase that is asymmetrically distributed. *Cell* 81, 611–620.
- Boyd, L., Guo, S., Levitan, D., Stinchcomb, D.T., and Kemphues, K.J. (1996). PAR-2 is asymmetrically distributed and promotes association of P granules and PAR-1 with the cortex in *C. elegans* embryos. *Development* 122, 3075–3084.
- Wodarz, A. (2002). Establishing cell polarity in development. *Nat. Cell Biol.* 4, E39–E44.
- Shulman, J.M., Benton, R., and St Johnston, D. (2000). The *Drosophila* homolog of *C. elegans* PAR-1 organizes the oocyte cytoskeleton and directs oskar mRNA localization to the posterior pole. *Cell* 101, 377–388.
- Wodarz, A., Ramrath, A., Grimm, A., and Knust, E. (2000). *Drosophila* atypical protein kinase C associates with Bazooka and controls polarity of epithelia and neuroblasts. *J. Cell Biol.* 150, 1361–1374.
- Petronczki, M., and Knoblich, J.A. (2001). DmPAR-6 directs epi-

- thelial polarity and asymmetric cell division of neuroblasts in *Drosophila*. *Nat. Cell Biol.* 3, 43–49.
14. Qiu, R.G., Abo, A., and Steven Martin, G. (2000). A human homolog of the *C. elegans* polarity determinant Par-6 links Rac and Cdc42 to PKCzeta signaling and cell transformation. *Curr. Biol.* 10, 697–707.
 15. Lin, D., Edwards, A.S., Fawcett, J.P., Mbamalu, G., Scott, J.D., and Pawson, T. (2000). A mammalian PAR-3-PAR-6 complex implicated in Cdc42/Rac1 and aPKC signalling and cell polarity. *Nat. Cell Biol.* 2, 540–547.
 16. Joberty, G., Petersen, C., Gao, L., and Macara, I.G. (2000). The cell-polarity protein Par6 links Par3 and atypical protein kinase C to Cdc42. *Nat. Cell Biol.* 2, 531–539.
 17. Grill, S.W., Gönczy, P., Stelzer, E.H., and Hyman, A.A. (2001). Polarity controls forces governing asymmetric spindle positioning in the *Caenorhabditis elegans* embryo. *Nature* 409, 630–633.
 18. Sulston, J.E., Schierenberg, E., White, J.G., and Thomson, J.N. (1983). The embryonic cell lineage of the nematode *Caenorhabditis elegans*. *Dev. Biol.* 100, 64–119.
 19. Kemphues, K. (2000). PARsing embryonic polarity. *Cell* 101, 345–348.
 20. Drewes, G., Ebneth, A., Preuss, U., Mandelkow, E.M., and Mandelkow, E. (1997). MARK, a novel family of protein kinases that phosphorylate microtubule-associated proteins and trigger microtubule disruption. *Cell* 89, 297–308.
 21. Goldstein, B., and Hird, S.N. (1996). Specification of the antero-posterior axis in *Caenorhabditis elegans*. *Development* 122, 1467–1474.
 22. Cheng, N.N., Kirby, C.M., and Kemphues, K.J. (1995). Control of cleavage spindle orientation in *Caenorhabditis elegans*: the role of the genes *par-2* and *par-3*. *Genetics* 139, 549–559.
 23. Schaefer, M., Shevchenko, A., and Knoblich, J.A. (2000). A protein complex containing Inscuteable and the G α -binding protein Pins orients asymmetric cell divisions in *Drosophila*. *Curr. Biol.* 10, 353–362.
 24. Gotta, M., and Ahringer, J. (2001). Distinct roles for G α and G $\beta\gamma$ in regulating spindle position and orientation in *Caenorhabditis elegans* embryos. *Nat. Cell Biol.* 3, 297–300.
 25. Schaefer, M., Petronczki, M., Dorner, D., Forte, M., and Knoblich, J.A. (2001). Heterotrimeric G proteins direct two modes of asymmetric cell division in the *Drosophila* nervous system. *Cell* 107, 183–194.
 26. Gotta, M., Abraham, M.C., and Ahringer, J. (2001). CDC-42 controls early cell polarity and spindle orientation in *C. elegans*. *Curr. Biol.* 11, 482–488.
 27. Tsou, M.F., Hayashi, A., DeBella, L.R., McGrath, G., and Rose, L.S. (2002). LET-99 determines spindle position and is asymmetrically enriched in response to PAR polarity cues in *C. elegans* embryos. *Development* 129, 4469–4481.
 28. Gönczy, P., Pichler, S., Kirkham, M., and Hyman, A.A. (1999). Cytoplasmic dynein is required for distinct aspects of MTOC positioning, including centrosome separation, in the one cell stage *Caenorhabditis elegans* embryo. *J. Cell Biol.* 147, 135–150.
 29. Hyman, A.A., and White, J.G. (1987). Determination of cell division axes in the early embryogenesis of *Caenorhabditis elegans*. *J. Cell Biol.* 105, 2123–2135.
 30. Tran, P.T., Marsh, L., Doye, V., Inoue, S., and Chang, F. (2001). A mechanism for nuclear positioning in fission yeast based on microtubule pushing. *J. Cell Biol.* 153, 397–411.
 31. Cassimeris, L., Pryer, N.K., and Salmon, E.D. (1988). Real-time observations of microtubule dynamic instability in living cells. *J. Cell Biol.* 107, 2223–2231.
 32. Sammak, P.J., and Borisy, G.G. (1988). Direct observation of microtubule dynamics in living cells. *Nature* 332, 724–726.
 33. Rodionov, V.I., Lim, S.S., Gelfand, V.I., and Borisy, G.G. (1994). Microtubule dynamics in fish melanophores. *J. Cell Biol.* 126, 1455–1464.
 34. Desai, A., and Mitchison, T.J. (1997). Microtubule polymerization dynamics. *Annu. Rev. Cell Dev. Biol.* 13, 83–117.
 35. Inoué, S., and Spring, K.R. (1997). *Video Microscopy - The Fundamentals*, Second Edition (New York: Plenum Press).
 36. Parsons, S.F., and Salmon, E.D. (1997). Microtubule assembly in clarified *Xenopus* egg extracts. *Cell Motil. Cytoskeleton* 36, 1–11.
 37. Brenner, S. (1974). The genetics of *Caenorhabditis elegans*. *Genetics* 77, 71–94.
 38. Oegema, K., Desai, A., Rybina, S., Kirkham, M., and Hyman, A.A. (2001). Functional analysis of kinetochore assembly in *Caenorhabditis elegans*. *J. Cell Biol.* 153, 1209–1226.
 39. Fire, A., Xu, S.Q., Montgomery, M.K., Kostas, S.A., Driver, S.E., and Mello, C.C. (1998). Potent and specific genetic interference by double-stranded RNA in *Caenorhabditis elegans*. *Nature* 391, 806–811.
 40. Dudley, N.R., Labbé, J.-C., and Goldstein, B. (2002). Using RNA interference to identify genes required for RNA interference. *Proc. Natl. Acad. Sci. USA* 99, 4191–4196.
 41. Edgar, L.G. (1995). Blastomere culture and analysis. *Methods Cell Biol.* 48, 303–321.

PAR Proteins Regulate Microtubule Dynamics at the Cell Cortex in *C. elegans*

Jean-Claude Labbé, Paul S. Maddox, E.D. Salmon, and Bob Goldstein

Table S1. Measure of Stability of Microtubules in Wild-Type, Polarity-Defective, and Spindle Positioning-Defective Embryos

Background	Measure of Microtubule Stability at the Cortex ^a			Difference (Anterior versus Posterior) ^b	P Value (Anterior versus Posterior) ^c
	Anterior	Posterior	Whole Embryo		
Wild-type	12.5 ± 0.9	10.6 ± 0.6	11.5 ± 0.7	17.9%	p = 0.03
<i>par-1(RNAi)</i>	9.4 ± 0.5	7.7 ± 0.3	8.6 ± 0.3	22.1%	p = 0.03
<i>par-2(RNAi)</i>	9.8 ± 0.7	9.5 ± 0.2	9.6 ± 0.4	3.2%	p = 0.62
<i>par-3(RNAi)</i>	8.6 ± 0.2	8.4 ± 0.2	8.5 ± 0.2	2.4%	p = 0.24
<i>par-2(RNAi); par-3(RNAi)</i>	9.0 ± 0.5	8.3 ± 0.2	8.7 ± 0.3	8.4%	p = 0.26
<i>Gα(RNAi)</i> ^d	10.5 ± 0.4	9.7 ± 0.9	10.1 ± 0.5	8.2%	p = 0.40
<i>Gα(RNAi); par-2(RNAi)</i> ^d	10.7 ± 0.8	9.8 ± 0.3	10.2 ± 0.6	9.2%	p = 0.19
<i>Gα(RNAi); par-3(RNAi)</i> ^d	8.7 ± 0.3	9.1 ± 1.0	8.9 ± 0.6	4.4%	p = 0.68

^a Microtubule stability was determined by cortical imaging of microtubule stability (CIMS) and was quantified by using method 2 (see the Experimental Procedures). Each value corresponds to the average apparent residence time of individual microtubules at the cortex (in seconds) ± the standard error of the mean across five embryos; because this method excludes dimly fluorescent segments, the apparent residence times are expected to be consistent underestimates of the real residence times of microtubules at the cortex (comparing this table with Table 1 suggests that this is the case). Despite the consistent underestimates, this method has the advantage of being more readily carried out, which facilitated repeated quantifications in blind experiments; these produced results consistent with those shown here. A total of 450 microtubules were monitored for each condition (225 for each side).

^b Represents the percentage of increase in stability at the cortex of anterior microtubules compared to posterior microtubules.

^c p values from paired Student's t tests between anterior and posterior average microtubule residence time at the cortex. Values were considered significantly different if p < 0.05.

^d *Gα(RNAi)* corresponds to the simultaneous disruption of the *goa-1* and *gpa-16* genes. See the main text for details.

Movie 1. Imaging Microtubules in *C. elegans* Embryos by Spinning-Disk Confocal Microscopy

Embryos from a strain expressing an α -tubulin::GFP fusion protein were visualized by spinning-disk confocal microscopy. This allowed the visualization of 0.7 μ m thick optical sections and yielded well-resolved, individual microtubules. In this movie, images were captured at a midplane (left panel) or cortical plane (right panel) of the embryo. This movie starts before pronuclear envelope breakdown and ends with cytokinetic furrow ingression. Anterior is oriented toward the bottom, and posterior is oriented toward the top. Frames were captured every 5 s and are played back at 12 frames/s.

Movie 2. Cortical Imaging of Microtubule Stability in Early *C. elegans* Embryos

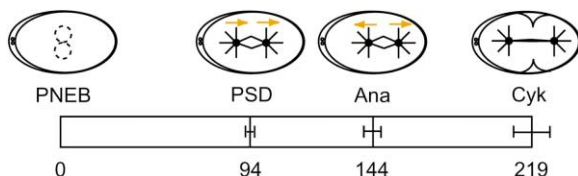


Figure S1. Timing of Events during Progression through the Cell Cycle

Timing of posterior spindle displacement (PSD), start of anaphase (Ana), and cytokinetic furrow ingression (Cyk) relative to pronuclear envelope breakdown (PNEB). The numbers at the bottom represent time in seconds relative to PNEB. Posterior spindle displacement occurs during metaphase and starts 94 ± 4 s after PNEB and ends at the start of anaphase. The error bars represent standard deviation over five embryos. Anterior is oriented toward the left.

The residence time of microtubules at the cortex can be determined by imaging microtubules in a cortical plane. In such movies, individual microtubules can be seen as individual dots or short line segments of fluorescence, and their stability at the cortex can be quantified by measuring the time during which a single microtubule is present in the plane of focus. This movie starts at pronuclear envelope breakdown and ends with cytokinetic furrow ingression. Anterior is oriented toward the left, and posterior is oriented toward the right. Frames were captured every 2 s and are played back at 12 frames/s.

Movie 3. Cortical Imaging of Microtubule Stability in the Anterior Cortex of the *C. elegans* Embryo

Two-fold magnification of the anterior cortex of the early *C. elegans* embryo. Filled arrowheads point to various individual microtubules that enter and leave the plane of focus in these time-lapse images; empty arrowheads indicate the position of these microtubules before and after they appear in the plane of focus. Residence time at the cortex can be calculated by determining the time (bottom right, in seconds) during which a given microtubule is visible at the cortex. Frames were captured every 2 s and are played back at 6 frames/s.

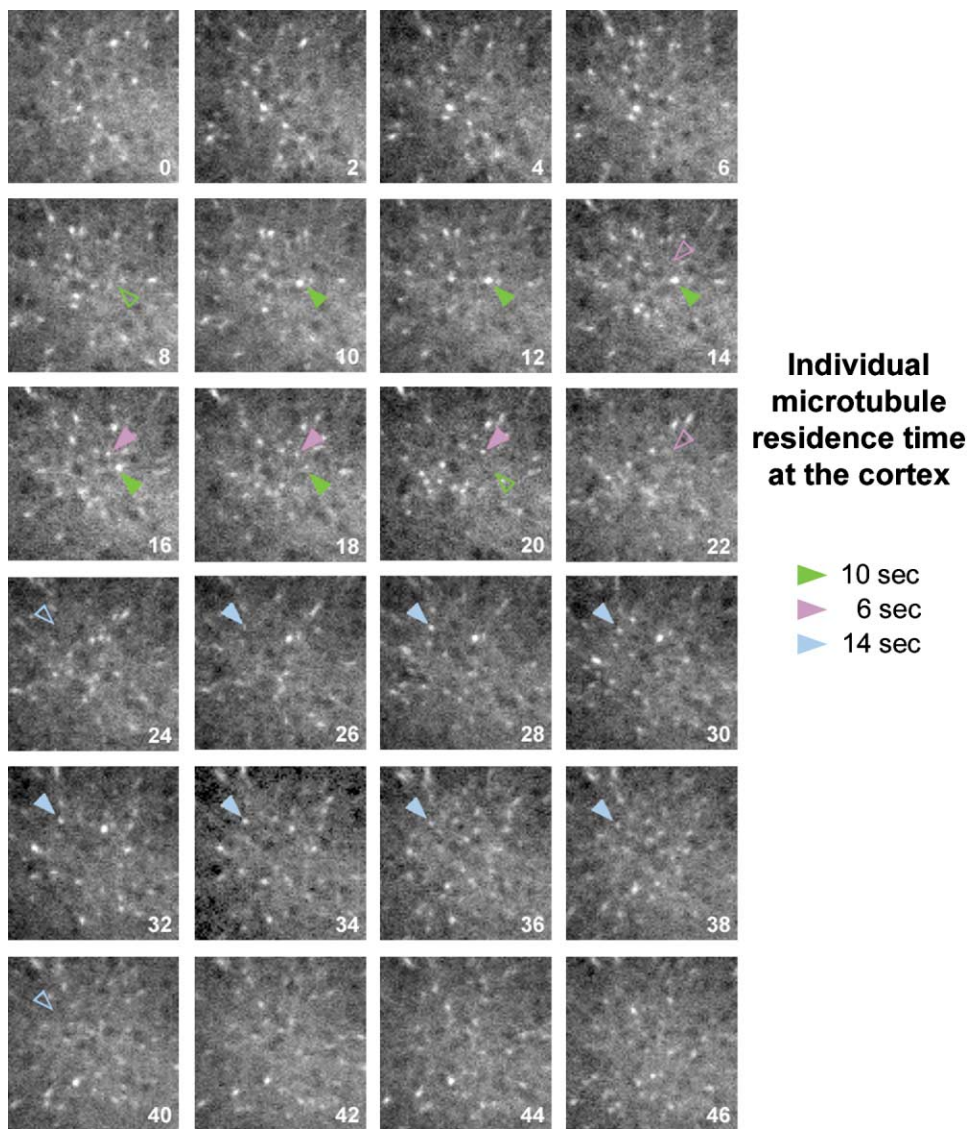


Figure S2. Time-Lapse Images of Microtubules at the Cortex

These consecutive time-lapse images illustrate individual microtubules at the anterior cortex of a wild-type embryo. Filled arrowheads point to various individual microtubules that enter and leave the plane of focus in these time-lapse images; empty arrowheads indicate the position of these microtubules before and after they appear in the plane of focus. The legend on the right reports the residence time of each microtubule.

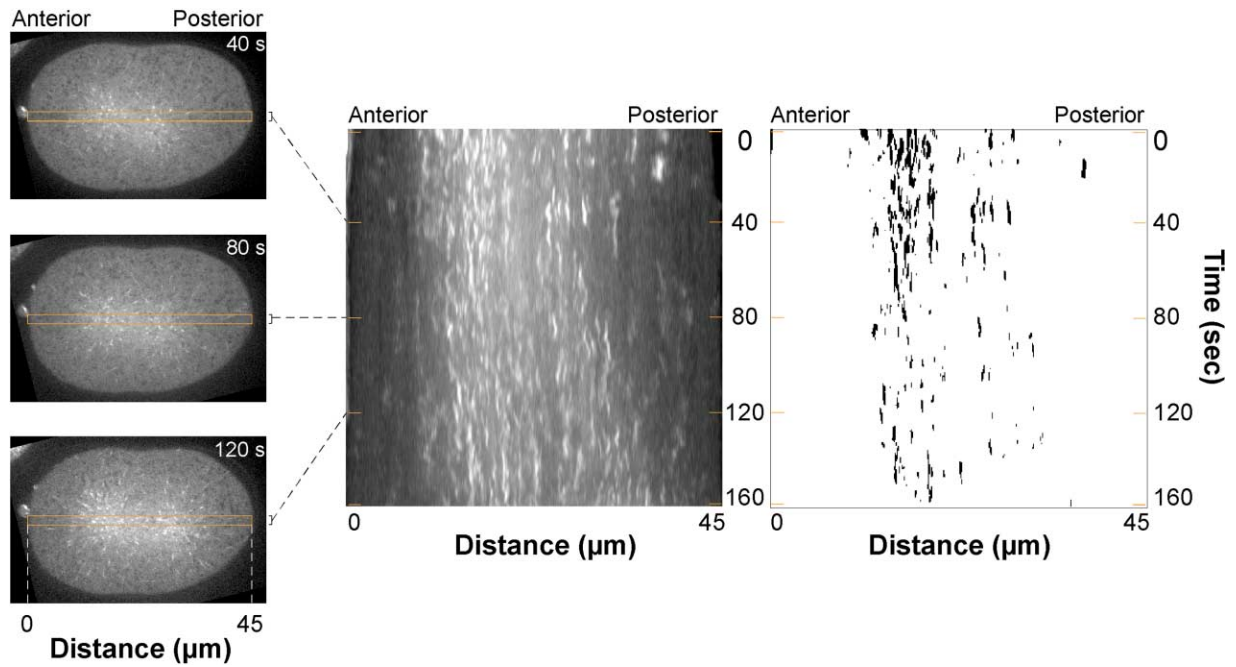


Figure S3. Kymocube Analysis of Microtubules at the Cortex of a Wild-Type *C. elegans* Embryo

A selected region along the anteroposterior axis of the embryo (left) was compressed down to four pixels and was displayed over time, starting from pronuclear envelope breakdown to the start of anaphase (middle). In these kymocubes, individual microtubules are visible as lines of fluorescence that persist during a given time. An automatic threshold function was applied to select the brightest events of fluorescence, thereby depicting individual microtubules (right). Residence time at the cortex can be determined by measuring the length in time of these individual microtubules.